minerals

MDPI

Article

DFT Study on the Interaction Between Flotation Agents and Lepidolite-1M Surfaces

Xujun Zhang [1,2], Guichun He [1,2,*] and Changzhen Du [1,2]

[1] Jiangxi Key Laboratory of Mining Engineering, Ganzhou 341000, China; 6720221218@mail.jxust.edu.cn (X.Z.); 6720230117@mail.jxust.edu.cn (C.D.)
[2] School of Resources Environmental Engineering, Jiangxi University of Science and Technology, Ganzhou 341000, China
* Correspondence: heguichun@jxust.edu.cn; Tel.: +86-13970766300

Abstract: The surface chemical properties of Lepidolite-1M crystals are closely related to their flotation properties. This paper uses density functional theory (DFT) to analyze the band structure, population, and state density of ideal Lepidolite-1M crystals. The results show that lepidolite-1M is an insulator, and its most probable positively charged active site is Al, and its negatively charged active sites are O and F. To further investigate the adsorption mechanism of Lepidolite-1M during comminution and flotation processes, we calculated the surface energy, population, state density, and differential charge density of its most common (001) surface. The results show that its surface energy is 0.9934 J/m^2, occurred in the valence electron configurations, population values, and bond lengths of the surface atoms. Furthermore, oxygen atoms on the (001) surface showed different activities, with F and O atoms in the lithium-rich region showing significant electron enrichment. Overall, our results demonstrated that anion collectors react mainly with the Al sites on the surface of Lepidolite-1M, and the cationic collectors and metal ion activators can be adsorbed on the surface of Lepidolite-1M to produce better trapping and activation capabilities.

Keywords: lepidolite-1M; lepidolite-1M (001) surface; density functional theory; electronic structure; surface properties

check for updates

Citation: Zhang, X.; He, G.; Du, C. DFT Study on the Interaction Between Flotation Agents and Lepidolite-1M Surfaces. *Minerals* **2024**, *14*, 1168. https://doi.org/10.3390/min14111168

Received: 9 October 2024
Revised: 28 October 2024
Accepted: 8 November 2024
Published: 18 November 2024

Copyright: © 2024 by the authors. Licensee MDPI, Basel, Switzerland. This article is an open access article distributed under the terms and conditions of the Creative Commons Attribution (CC BY) license (https://creativecommons.org/licenses/by/4.0/).

1. Introduction

Lithium mica K{$Li_2Al_1[Al_2Si_4O_{10}](OH,F)_2$} is part of a series between poly-lithium and tri-lithium minerals, featuring a T-O-T layered structure with potassium connecting atoms. It is of interest due to its high lithium content (up to 7.70% Li_2O) [1–4]. Due to isomorphic substitution in lithium mica, various metals such as Rb and Cs can exist in isomorphic forms, making it a major source of metals like rubidium and cesium [5,6]. Currently, the most widely used method for lithium mica recovery is flotation. It is crucial to separate highly floatable minerals such as feldspar, quartz, and white mica during flotation. Thus, developing highly selective flotation reagents for the more effective separation of lithium mica from other silicate minerals is of significant importance. The properties of minerals are closely related to their selectivity, possessing "genetic" characteristics, which significantly impact sorting indicators [7]. Therefore, exploring the "genes" of lithium mica minerals can provide valuable references and guidance for the study of lithium mica flotation behavior and the development of flotation reagents.

The Lepidolite-1M structure, which is a common configuration among a variety of lepidolite structures and rich in LiO_2, is characterized by significant octahedral order and considerable tetrahedral distortion. It has a relatively low level of duality in arrangement compared to the commonly occurring 2M2 structure [8,9]. In the lepidolite structure, between two layers of tetrahedral silica opposite the apex oxygen, there lies a layer of octahedral alumina (comprising three octahedra at positions M1, M2, and M3) [10,11]. In Lepidolite-1M, these octahedra contain various different cations, including Li^+, Al^{3+}, and

smaller substitutions. Extensive research has been conducted on the structural order of lepidolite. F. Sartori compared the Lepidolite-1M structure with the Lepidolite-2M2 structure and found no significant differences in chemical composition and structural parameters [12]. Stephen Guggenheim refined the 1M and 2M2 mica structures at multiple locations to establish ideal and sub-group symmetrical cation ordering schemes [13]. Chiara Elmi and others calculated the crystal chemistry and surface configurations of two polylithionite-1M crystals, finding that increased Li content on or near the (001) cleavage surface indicates a tendency for cleavage near lithium-rich areas [14].

Quantum chemical calculations have become a crucial basis for studying the structure of mineral crystals and the mechanisms of reagent action on mineral surfaces. Density functional theory is extensively used in researching the structure of mineral crystals and the interaction mechanisms between reagents and mineral surfaces [15–18]. Density functional theory has been widely applied in studying the crystal structure of minerals and the mechanisms of interaction between agents and mineral surfaces. Although extensive research has been conducted on the flotation separation of lithium mica, studies on its crystal chemical properties are not yet comprehensive. Defined by Rieder et al. as $^{[iv]}Si^{4+}_{-1}{}^{[vi]}Li_{-1}{}^{[iv]}Al^{[vi]}Fe^{2+}$, Polylithionite [$KLi_2AlSi_4O_{10}(F,OH)_2$] is a lithium-rich unit located near the trilithium polylithium ion connection in the trioctahedral mica [19]. This paper, utilizing the CASTEP module of Materials Studio software, modified and doped the Lepidolite-1M crystal, following Stephen Guggenheim and others, to obtain an ideal Lepidolite-1M crystal conforming to the trioctahedral configuration and composed of TOT-type structures [13]. Based on first principles, the energy bands, populations, and density of states of the ideal Lepidolite-1M crystal were calculated. The optimized Lepidolite-1M unit cell was then cut along the Miller index (001) direction, and its relaxation, population, density of states, and differential charge density were analyzed. In-depth analysis of the structure and surface characteristics of Lepidolite-1M crystals provides a reference for the development of flotation reagents for lithium mica.

2. Simulation and Calculation Methods

2.1. Construction and Optimization of Lithium Mica Cells

The crystal cell structure of lithium mica was geometrically optimized using the CASTEP module of Materials Studio 2016 software. The modified Lepidolite-1M crystal belongs to the monoclinic crystal system and is a TOT-type layered silicate mineral. Its space group is C2/m, with cell parameters: a = 5.209, b = 9.011, c = 10.149, $\alpha = \gamma = 90°$, $\beta = 100.77°$. Basic parameter set: ultralight pseudopotentials and BFGS algorithm were used. The self-consistent accuracy was set to 2×10^{-6} eV/atom, interatomic forces at 0.05 eV/atom, the internal stress convergence threshold for interatomic interactions at 0.1 GPa, the maximum atomic displacement convergence threshold at 2×10^{-4} nm, and a maximum of less than 1000 iteration steps. All calculations were performed in reciprocal space.

The lithium mica crystal cell was geometrically optimized, comparing the single-point energy and structural parameters under different computational conditions to determine the best computational simulation parameters, focusing on the analysis of exchange-correlation functionals, k-point sampling density, and cutoff energy. Initially, under the exchange-correlation function GGA-PBE, tests were conducted on k-point sampling density and cutoff energy, as shown in Figure 1. The results indicate that when the k-point sampling density exceeds $4 \times 4 \times 3$, the energy change in the crystal cell model is minimal, making this parameter appropriate. When the cutoff energy exceeds 380 eV, its impact on the crystal cell energy is small, and the total energy of the crystal cell tends to stabilize, thus the optimal cutoff energy parameter for calculation is 380 eV.

The cell parameters and single-point energies of Lepidolite-1M were investigated using different exchange-correlation functionals, with the results presented in Table 1. The cell parameters are as follows: a = 5.209 Å, b = 9.011 Å, c = 10.149 Å. Analysis of the results in Table 1 reveals that the cell parameters obtained through geometrical optimization using

GGA-PBE exchange-correlation generalized functionals most closely match the reference values. Consequently, GGA-PBE exchange-correlation generalized functionals are selected for the structural optimization and property calculations of lithium mica.

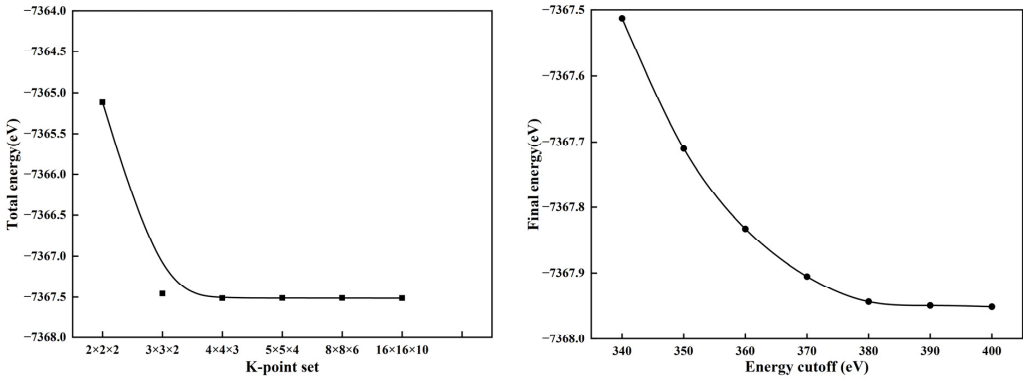

(**a**) (**b**)

Figure 1. (**a**) Results at different k-point sampling densities; (**b**) Results at different cutoff energies.

Table 1. Lepidolite-1M cell parameters calculated with different exchange-correlation floods.

Exchange Functions	a/Å	b/Å	c/Å	β/°	Difference/%
GGA-PBE	5.2026	8.9795	10.1856	100.4217	0.2778
GGA-PRBE	5.2036	8.7835	10.1784	100.3992	0.9730
GGA-PW91	5.2009	8.9757	10.1930	100.4144	0.3268
GGA-WC	5.1967	8.9670	10.2106	100.4027	0.4436
GGA-PBESOL	5.1999	8.9736	10.1976	100.4205	0.3562
LDA-CA-PZ	5.1552	8.8965	10.3716	100.3177	1.4988

The optimized crystal cell parameters of Lepidolite-1M are a = 5.1785 Å, b = 8.9838 Å, c = 10.2442 Å, α = 90.00°, β = 100.77°, γ = 90°. The XRD patterns of the optimized cell model were compared with those of pure lithium mica minerals from the Yichun region of China (Figure 2). The simulated XRD characteristic peaks essentially match those in the detected spectrum. Therefore, the Lepidolite-1M model corresponds to the actual situation, and the analysis of the model's crystal structure properties can represent the characteristics of the lithium mica mineral.

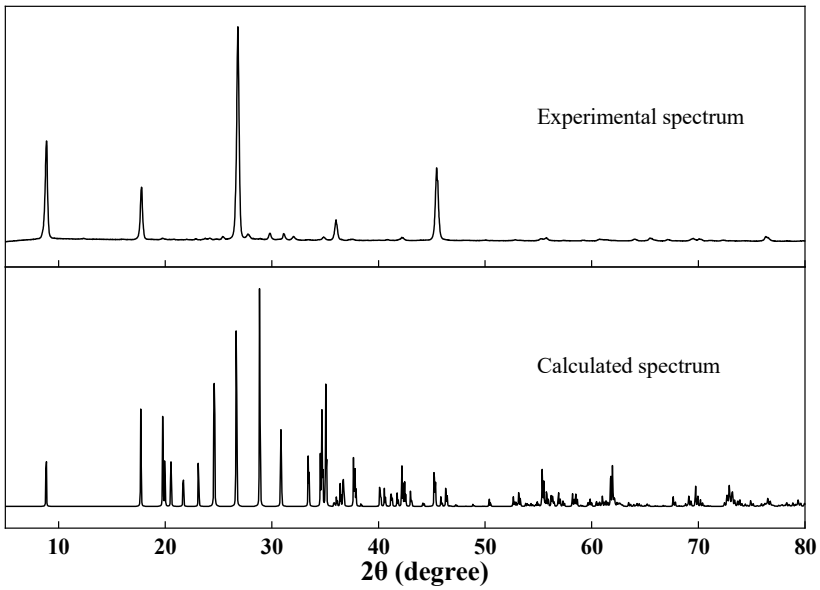

Figure 2. Actual lithium mica XRD pattern and Lepidolite-1M simulated XRD pattern.

2.2. Calculation of Surface Energy

The creation of a new surface in a material requires work to be performed by an external force, breaking the chemical bonds between surface atoms and their neighbors. Half of the work needed for this process is defined as the surface energy. The lower the surface energy, the more stable the properties of the surface. The surface energy is calculated according to Equation (1): [20]

$$E_{surf} = \frac{\left[E_{slab} - \frac{N_{slab}}{N_{bulk}} \cdot E_{bulk}\right]}{2A} \quad (1)$$

In the formula, E_{surf} represents the surface energy (J/m^2), E_{slab} is the total energy of the surface structure (J/m^2), N_{bulk} is the total energy of the mineral cell (J/m^2), N_{slab} is the number of atoms in the surface structure, N_{bulk} is the number of atoms in the optimized mineral cell, and A denotes the area of the calculated surface (m^2).

2.3. Surface Modeling

According to Frank C. Hawthorne et al., the (001) surface is the most stable surface of Lepidolite-1M [11]. Therefore, this paper cuts the crystal cell along the Miller index (001) direction after optimization. When the number of cut layers of Lepidolite-1M is 3 and the vacuum layer thickness is 1.5 nm, the cut surface is sufficient to maintain stable surface properties, and the interference between the top and bottom surfaces is minimal. If the number of cut layers and vacuum layer thickness continue to increase, the stability of the surface changes little, but the calculation time significantly lengthens. Therefore, this paper chooses a (001) surface slab model with 3 cut cell layers and a vacuum layer thickness of 1.5 nm. The optimized Lepidolite-1M crystal and the optimized Lepidolite-1M (001) surface are shown in Figure 3.

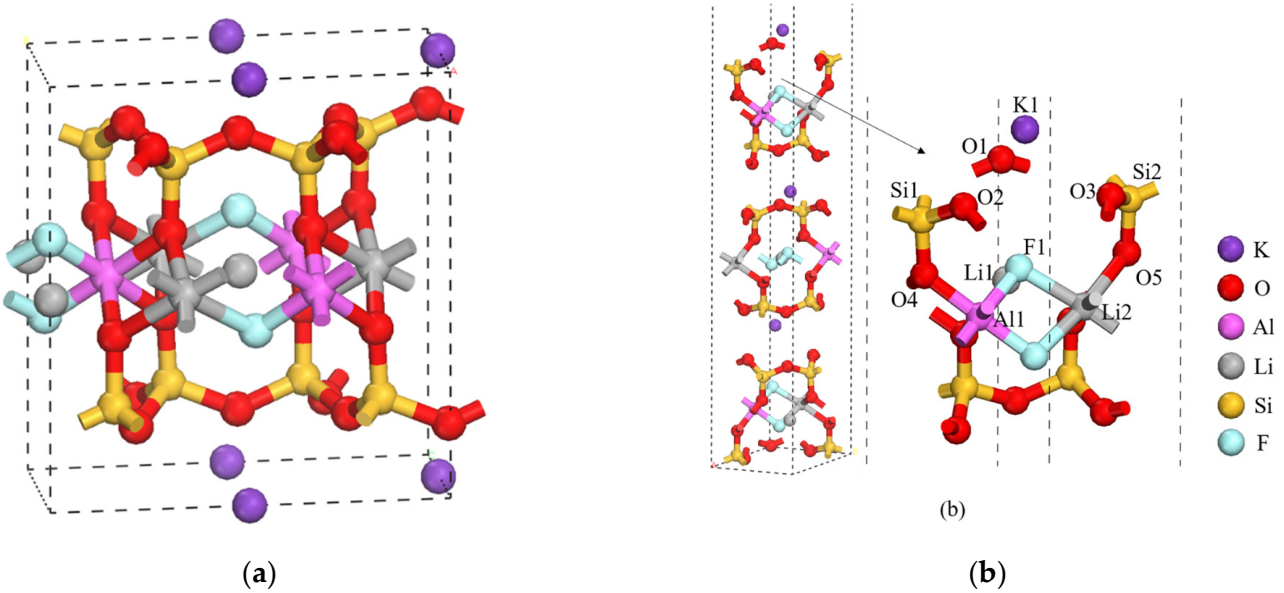

Figure 3. (**a**) Lepidolite-1M cell; (**b**) Lepidolite-1M (001) surface.

3. Calculation Results and Discussion

3.1. Lepidolite-1M Crystal Analysis

3.1.1. Mulliken Population Analysis

The atomic population results for Lepidolite-1M are shown in Table 2. As shown: In Lepidolite-1M, the main positively charged atoms are Li, Al, K, and Si, while the negatively charged atoms are O and F.

Table 2. Mulliken population of atoms in lepidolite-1M.

Species	s	p	d	Total (e)	Charge (e)
Li	2.00	0.31	0.00	2.31	0.70
O1	1.83	5.29	0.00	7.12	−1.12
O2	1.84	5.26	0.00	7.11	−1.11
O3	1.85	5.21	0.00	7.07	−1.07
F	1.95	5.70	0.00	7.65	−0.65
Al	0.50	0.91	0.00	1.40	1.60
Si	0.69	1.36	0.00	2.04	1.96
K	2.02	5.55	−0.02	7.55	1.45

As can be seen from Table 2, the positively charged atoms in Lepidolite-1M are mainly Al, Si, K, and Li, and the negatively charged atoms are O and F. The optimized Al atom's valence electron configuration is Al $3s^{0.50}p^{0.91}$, with the s orbital losing 1.50 units of electrons and the p orbital losing 0.09 units, mainly in the 3s orbital, resulting in a charge of 1.60 e for Al. The optimized Si atom's valence electron configuration is Si $3s^{0.69}p^{1.36}$, with the s orbital losing 1.31 units of electrons and the p orbital losing 0.64 units, mainly in the 3s orbital, resulting in a charge of 1.96 e for Si. The optimized K atom's valence electron configuration is K $3s^{2.02}3p^{5.55}3d^{-0.02}$, with a localized electron count of 7.55 e, losing 2.45 electrons, and a charge of +1.45 e for K, indicating it is an electron donor, primarily due to the removal of electrons from K's d orbitals. In the optimized state, O has three valence electron configurations; the first configuration is O $2s^{1.83}2p^{5.29}$, where the s orbital loses 0.17 electrons and the p orbital gains 1.29 electrons, primarily due to the p orbital, resulting in a charge of −1.12 e, the second configuration is O $2s^{1.84}2p^{5.26}$, where the s orbital loses 0.16 electrons and the p orbital gains 1.26 electrons, with the main gain in the p orbital, leading to a charge of −1.11 e, the third configuration is O $2s^{1.85}2p^{5.21}$, with the s orbital losing 0.15 electrons and the p orbital gaining 1.21 electrons, mainly in the p orbital, resulting in a charge of −1.07 e. The valence electron configuration of the optimized F atom is F $2s^{1.95}2p^{5.70}$. The s orbital loses 0.05 electrons, and the p orbital gains 0.70 electrons, primarily in the p orbital, resulting in a charge of −0.65 e.

The closer the mineral Mulliken bond population value is to 0, the stronger the ionic character of the bond; the closer to 1, the stronger the covalent character [21]. The bond population of Lepidolite-1M is shown in Table 3.

Table 3. Mulliken population of bonds in 1M.

Bond	Population	Length (Å)
Li-O	0.08–0.11	2.101–2.118
Al-O	0.35	1.908–1.910
Si-O	0.59–0.73	1.588–1.648
F-Al	0.29	1.852
Li-F	0.10–0.11	2.085–2.095

As seen from Table 3, in the Lepidolite-1M crystal, Al-O, Si-O, and Li-F bonds have different population values and bond lengths due to the complex structure of Lepidolite-1M; the Li-O bond in Lepidolite-1M has the strongest ionic nature, making it more likely to form ionic bonds, while the Si-O bond has stronger covalent character. Therefore, during milling and flotation, the Li-O bond is most likely to break, followed by Li-F, F-Al, Al-O, and lastly Si-O bonds. In the flotation process, the dissociation of the Lepidolite-1M surface exposes K^+ and $[SiO_4]^-$. As K^+ dissolves in the slurry, the Lepidolite-1M surface becomes negatively charged and readily binds with hydroxyl groups [22]. At the same time, due to the high electronegativity of F on the surface of Lepidolite-1M, it replaces the hydroxyl groups at the surface interface and enters the Lepidolite-1M lattice. The O on the Lepidolite-1M surface also readily adsorbs electron-deficient groups in the solution to form hydrogen bonds. Additionally, the relative density of multivalent metal cations and anions on the mineral surface is relatively small, resulting in negative charges over a wide pH range and a low zero charge point, consistent with the conclusions obtained in the literature [23].

3.1.2. Energy Band Analysis

Calculated from Figure 4, it is known that the energy band gap width of Lepidolite-1M is 5.506 eV, thus classifying Lepidolite-1M as an insulator.

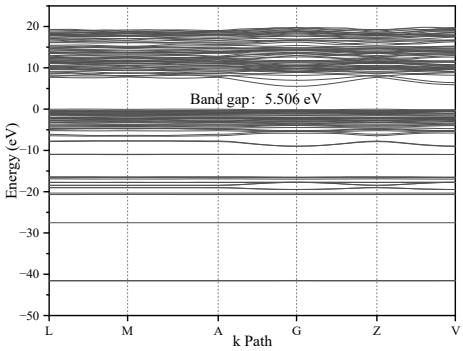

Figure 4. Energy band diagram of the Lepidolite-1M crystal.

Figure 5 shows the partial density of states for each atom of Lepidolite-1M and the total density of states. From Figure 5, it is known that the energy bands of Lepidolite-1M are mainly divided into five parts; the first part is between −44 and −41 eV, primarily composed of Li's s orbitals; the second part is between −28 and −26 eV, entirely composed of K's s orbitals; the third part is between −22 and −15 eV, mainly consisting of O and F's s orbitals, with Si and Al's s and p orbitals also contributing slightly to this valence band; the top valence band is mainly composed of O and F's p orbitals, with a minor contribution from Si and Al's s and p orbitals; the conduction band level mainly includes contributions from Si and Li's s and p orbitals, with a small amount from Al. The electronic activity is strongest near the Fermi energy level [24]. The p orbitals of O contribute the most to the density of states near the Fermi energy level, making O the most active atom in Lepidolite-1M, followed by F, Si, and Al. However, population analysis shows that Li+ and K+ dissolve in water during flotation, and the Si-O bond is harder to break than the Al-O bond during crushing and milling. Therefore, Al is the most probable positively charged active site on the surface of Lepidolite-1M, and O is the most probable negatively charged active site on the surface of Lepidolite-1M. Additionally, the population distribution indicates that there are three different valence electron configurations of O in Lepidolite-1M, namely O1, O2, and O3. From the partial density of states of these three types of O, it is evident that the p orbitals of O3 contribute the most to the density of states near the Fermi energy level, followed by O1's p orbitals, and O2's p orbitals contribute the least. Therefore, among these three types of O, the activity decreases in the order of O3, O1, and O2.

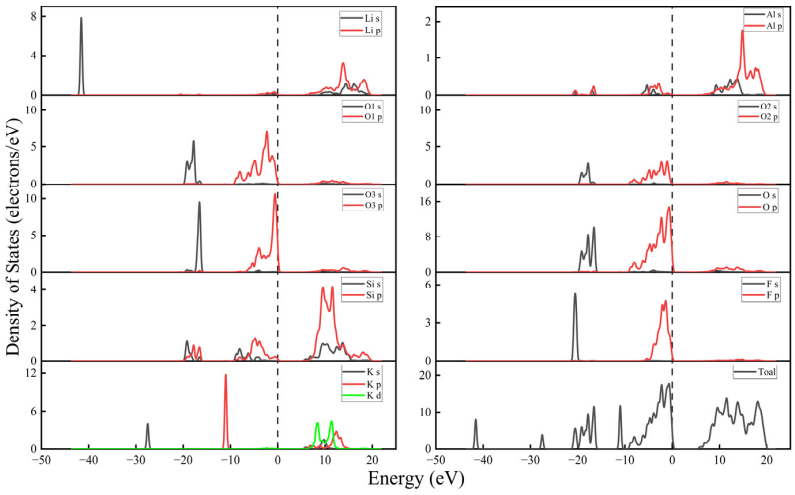

Figure 5. Lepidolite-1M total density of states map and partial density of states for each atom.

3.2. Surface Characterization of Lepidolite-1M (001)

3.2.1. Surface Energy of the Lepidolite-1M (001) Surface

The surface energy of the optimized Lepidolite-1M (001) surface is calculated according to Formula (1), and the results are shown in Table 4. The surface energy of the constructed Lepidolite-1M (001) surface is 0.9934 J/m^2.

Table 4. The computational items of the surface energy of Lepidolite-1M(001).

Calculation Term	E_{bulk} /(10^{-19}J)	E_{slab} /(10^{-19}J)	$\frac{E_{slab}}{E_{bulk}}$	$2A$ /(10^{-20}m^2)	E_{surf} /(J m^{-2})
calculated value	−11,806.15	−35,414.52	3	47.18	0.9934

3.2.2. Lepidolite-1M (001) Faceted Population Analysis

Due to the relative displacement of surface atoms and changes in coordination number, the outer electrons of the atoms change, resulting in altered bond lengths. Table 5 presents the Mulliken population distribution of surface atoms on the Lepidolite-1M (001) facet. Compared to the bulk phase of Lepidolite-1M, the outer electrons of all surface atoms on the Lepidolite-1M (001) facet, except for Li, O3 and F1, have changed. The valence electron configuration of Al1 changes to Al3s$^{0.50}$p$^{0.90}$. Its s orbital remains unchanged, but the p orbital loses 0.01 e more electrons than in the bulk phase, with a resulting charge of 1.6 e. Si has only one type of valence electron configuration, Si3s$^{0.70}$3p$^{1.36}$. Compared to the bulk phase, its s orbital loses an additional 0.01 units of electrons with no change in the p orbital, resulting in a charge of 1.94 e. The valence electron configuration of K changes to K3s$^{2.22}$3p$^{5.85}$3d$^{0.01}$. Compared to the bulk phase, its s orbital loses 0.2 units fewer electrons, the p orbital loses 0.3 units fewer electrons, and the d-orbital loses 0.03 units fewer electrons, resulting in a charge of 0.92 e. The valence electron configurations of the remaining five surface O atoms are all different: O2s$^{1.84}$2p$^{5.28}$, O2s$^{1.85}$2p$^{5.26}$, O2s$^{1.83}$2p$^{5.29}$, O2s$^{1.86}$2p$^{5.21}$, and O2s$^{1.86}$2p$^{5.20}$. Compared to the bulk phase, the changes in surface O are minor; both the s and p orbitals either gain or lose a small number of electrons or remain unchanged, with the charge variation not exceeding 0.01 e.

Table 5. The atom Mulliken population of Lepidolite-1M (001) surface.

Species	s	p	d	Total (e)	Charge (e)
Li1	2.00	0.31	0.00	2.30	0.70
Li2	2.00	0.31	0.00	2.30	0.70
O1	1.84	5.28	0.00	7.12	−1.12
O2	1.85	5.26	0.00	7.11	−1.11
O3	1.83	5.29	0.00	7.12	−1.12
O4	1.86	5.21	0.00	7.06	−1.06
O5	1.86	5.20	0.00	7.06	−1.06
F1	1.95	5.70	0.00	7.65	−0.65
Al	0.50	0.90	0.00	1.40	1.60
Si1	0.70	1.36	0.00	2.06	1.94
Si2	0.70	1.36	0.00	2.06	1.94
K1	2.22	5.85	0.01	8.08	0.92

According to Table 6, the bond population values for Li1-O and Li2-O bonds do not change significantly, but the overall bond lengths increase, leading to weaker bonds. The bond populations of Al1-O4 and Al1-O5 are both 0.33, with nearly equal bond lengths. Compared to the bulk phase, the decrease in population values and increase in bond lengths indicate enhanced ionic character. The bond populations for Al1-F1 and Li1-F1 do not change significantly, but the latter's bond length increases noticeably, indicating that Li-F bonds exhibit stronger ionic character than Al-F bonds after cleavage. The bond population values and lengths of Si-O bonds also change. Among the eight Si-O bonds, except for Si1-O2 and Si2-O2 being identical, the rest show slight variations in both population values and lengths, similar to the variety of Si-O bonds in the bulk phase. This indicates that there is no significant reconstruction of the surface Si-O bonds in Lepidolite-1M after cleavage. On the surface of Lepidolite-1M, the Li1-O5 bond is most likely to break, followed by Li1-O1, Li2-O4, Li1-F1, Al1-F1, and finally, the Si-O bonds. On the surface of Lepidolite-1M, Li-O bonds still

maintain the strongest ionic character, while Si-O bonds retain the strongest covalent character, consistent with the bulk phase. However, on the Lepidolite-1M (001) surface, the bond lengths of Li-O bonds are longer compared to the bulk phase, with increased ionic character making dissociation more likely. Robert et al. [25] indicated that the higher the bond-valence sum received by the non-silicate O3 from its three adjacent cations (Al^{3+} and Li) at the octahedral sites, the lower the bond valence exchanged within the hydroxyl, and therefore the lower the wavenumber of the O-H stretching band. According to their investigations, the O-H bands obtained by hydration of the Lepidolite-1M (001) facets modeled in this study under flotation conditions belong to the TRI-7 band, which are due to a seven-charge environment (hydroxyl bonded to $Al^{+}{}_{2}Li$). This results in lithium mica carrying a negative charge over a wide pH range and having a very low point of zero charge. Consequently, the flotation effect of lithium mica in the dodecylamine system is stronger than in the sodium oleate system, in line with theoretical literature [26].

Table 6. The bond Mulliken population of Lepidolite-1M (001) surface.

Bond	Population	Length (Å)
Li1-O4	0.09	2.152
Li1-O5	0.08	2.163
Li2-O4	0.09	2.148
Li2-O5	0.10	2.157
Al1-O4	0.33	1.931
Al1-O5	0.33	1.938
Si1-O1	0.59	1.652
Si1-O2	0.58	1.660
Si1-O3	0.58	1.653
Si1-O4	0.76	1.579
Si2-O1	0.58	1.652
Si2-O2	0.58	1.660
Si2-O3	0.59	1.653
Si2-O5	0.76	1.576
Al1-F1	0.28	1.874
Li1-F1	0.10	2.166

3.2.3. Density of States Analysis of the Lepidolite-1M (001) Surface

Figure 6 shows the density of states (DOS) graph for the surface atoms of the Lepidolite-1M (001) facet.

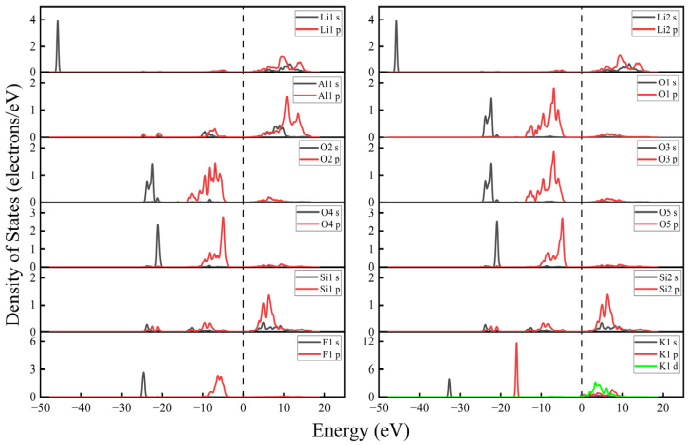

Figure 6. Density map of each atomic state in the surface layer of Lepidolite-1M (001).

According to Figure 6, the band structure of the Lepidolite-1M (001) surface is similar to the bulk phase, mainly divided into five parts. Between −47 and −45 eV, it is composed almost entirely of the s orbitals of Li1 and Li2. Between −34 and −32 eV, it is composed solely of the s orbital of K1. Between −20 and −26 eV, the bands are mainly composed of the s orbitals of F1, O1, O2, O3, O4, and O5. Additionally, the s and p orbitals of Si1, Si2, and Al1 also contribute slightly to this part of the valence band. The top part of the valence band is primarily composed of the p orbitals of all surface O atoms and F1, with a minor contribution from the s and p orbitals of Si and Al. In the conduction band energy levels between 0 and 20 eV, except for minimal participa-

tion by surface O, all atoms contribute with their orbitals. Additionally, the p orbitals of F replace those of O in contributing the maximum state density near the Fermi level, making F1 the most active atom among the surface atoms of Lepidolite-1M (001). The five surface oxygen atoms contribute differently to the state density near the Fermi level, indicating varied reactivities. The contributions of these five oxygen atoms, in terms of state density near the Fermi level, are as follows: O4 ≈ O5 > O3 ≈ O1 > O2, that is, the O in the alumina octahedron region > O near Li ≈ surface O > O near Al.

3.2.4. Differential Charge Density Map of the Lepidolite-1M (001) Surface

Figure 7 shows the differential charge density map of the surface electrons of Lepidolite-1M (001), where the red areas indicate electron depletion, blue areas indicate electron enrichment, and white areas indicate almost no change in electron density.

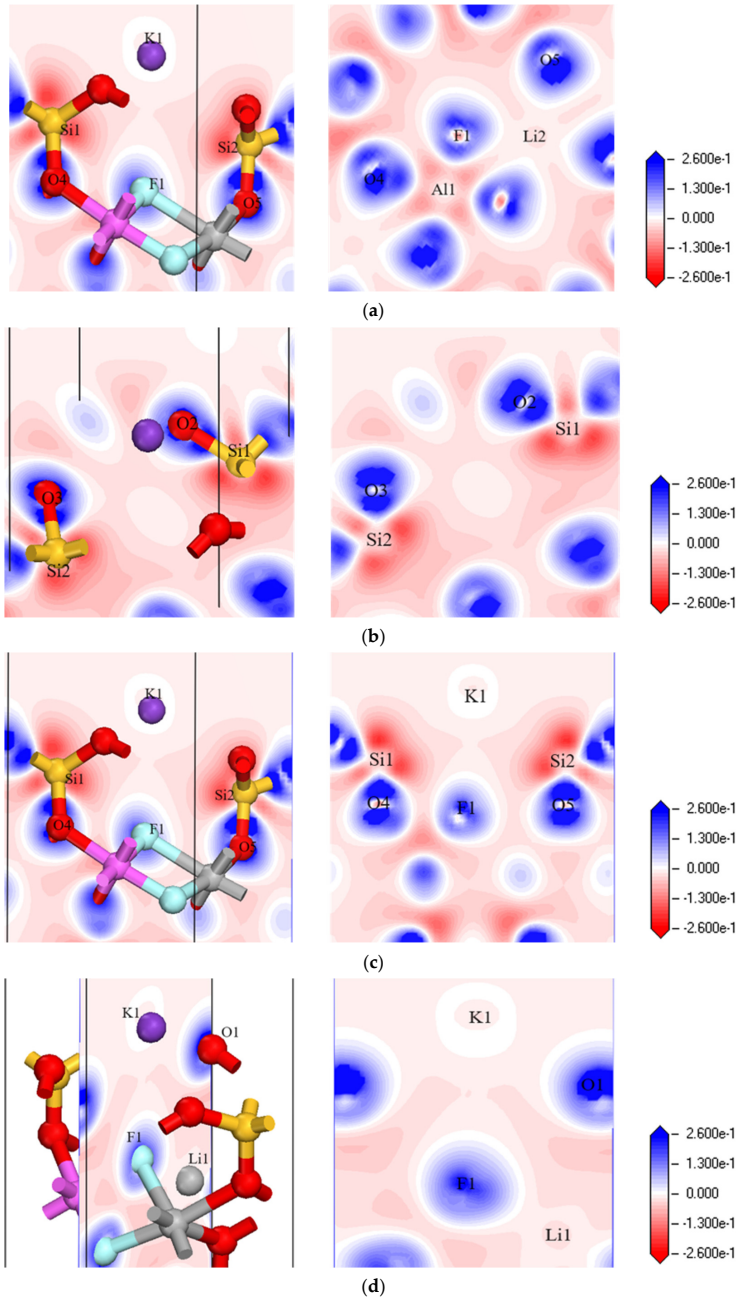

Figure 7. Lepidolite-1M (001) surface differential density charge of (**a**) O4-Al1-F1-Li2-O5, (**b**) Si1-O2, Si2-O3, (**c**) Si1-O4, Si2-O5, K1, (**d**) K1, F1, O1, Li1.

From Figure 7a, it is observed that the internal charge differential density of O4, O5, and F1 is deep blue with the periphery being white. This indicates significant electron enrichment and increased charge density in O4, O5, and F1, consistent with their high electronegativity. The electron enrichment of F1 is weaker, aligning with the results of Mulliken population analysis for the surface atoms of Lepidolite-1M (001); in the figure, the charge density around Li2 is visibly lower than that around Al1, and the electron cloud distribution in the Li2-F1 bond is not prominent, indicating that the ionic character of the bond is higher than that of the Al1-F1 bond, with poorer stability compared to other bonds, consistent with Mulliken bond population analysis. Figure 7b,c reveal a strong overlap of electron clouds between Si-O atoms, displaying characteristics of covalent bonds, which aligns with the Mulliken bond analysis results. In Figure 7d, the periphery of K1 is light red, indicating a significant loss of electrons from K1 and their transfer to O1, consistent with the poor electronegativity of K and its weak ability to bind valence electrons.

4. Discussion

Based on the above calculations, it is known that the positively charged active sites on the surface of Lepidolite-1M are mainly Al. It is predicted that Lepidolite-1M easily interacts with anionic collectors containing functional groups such as -COOH, -CONHOH, -OSO2H, which readily undergo chemical reactions with Al. However, according to its density of states, the activity of positively charged sites like Li and Al is low. Therefore, when using such anionic collectors, their collecting performance may be poor. The negatively charged active sites in Lepidolite-1M are O and F, and their activity is relatively high. Thus, it is predicted that cationic collectors such as amine collectors, as well as metal ion activators like Cu^{2+}, can adsorb onto the Lepidolite-1M surface, mainly interacting with the lithium-rich regions on the (001) surface of Lepidolite-1M. Due to the high activity of O, cationic collectors are likely to exhibit better collecting performance, and metal ions may demonstrate a more effective activation effect.

5. Conclusions

In this paper, density functional theory (DFT) is applied to the calculation of chemical properties on the surface of lepidolite crystals in order to infer the flotation properties of lepidolite by DFT. The energy band structure, layout, and density of states of an ideal Lepidolite-1M crystal are analyzed by simulation. The surface energy, Mulliken population analysis, partial density of states, and differential charge density were further calculated for its most common (001) surface. The results are as follows:

(1) The band and state density analysis of Lepidolite-1M crystals indicates that the band gap of Lepidolite-1M is 5.506 eV, which classifies it as an insulator. The bands are mainly divided into five parts, with the p orbitals of O contributing most to the state density near the Fermi level, making O the most active atom in Lepidolite-1M crystals and the most likely negatively charged active site.

(2) State density analysis shows that the activity of several O atoms in the outer layer of the silicate octahedron on the (001) plane differs, with their contribution to the state density near the Fermi level in the order of: O in the alumina octahedron region > O near Li ≈ outer O > O near Al.

(3) Differential charge density maps show alternating electron-deficient and electron-rich sites on the (001) plane, but with varying degrees of electron gain and loss. O and F in the lithium-rich region on the silicate octahedron show substantial electron enrichment and increased charge density, consistent with their strong electronegativity. Al and Li on the silicate octahedron show electron deficiency and significantly lower charge density, with electron cloud distribution around Li less pronounced, indicating stronger ionic nature of bonds and less stability compared to other bonds; meanwhile, electron cloud overlap between Si-O atoms is stronger, showing characteristics of covalent bonds.

(4) Based on the mineral genetic characteristics, it is predicted that Lepidolite-1M will readily interact with anionic collectors containing functional groups such as -COOH, -CONHOH, -OSO2H, which easily react with Al, although the collection performance may be poor. Cationic collectors such as amine collectors and metal ion activators such as Cu^{2+} are predicted to adsorb on the surface of Lepidolite-1M and exhibit good collecting and activating capabilities.

Author Contributions: Data curation, Visualization, Writing—review and editing, X.Z.; Conceptualization, Methodology, Supervision G.H.; Software, Data curation, C.D. All authors have read and agreed to the published version of the manuscript.

Funding: This work was supported by the National Key Scientific Research Projects of China (No. 2023YFC2908200) and Key Research and Development Program of Jiangxi Province (No. 20203BBGL73231).

Data Availability Statement: Data are contained within the article.

Conflicts of Interest: The authors declare no conflicts of interest.

References

1. Levinson, A.A. Studies in the mica group relationship between polymorphism and composition in the muscovite-lepidolite series. *Am. Mineral.* **1953**, *38*, 88–107.
2. Garrett, D.E. *Handbook of Lithium and Natural Calcium Chloride*; Mining Engineering: Ojai, CA, USA, 2004.
3. Christmann, P.; Gloaguen, E.; Labbé, J.-F.; Melleton, J.; Piantone, P. *Chapter 1—Global Lithium Resources and Sustainability Issues*; Elsevier: Amsterdam, The Netherlands, 2015; Volume 1, pp. 1–40.
4. Li, H.; Eksteen, J.; Kuang, G. Recovery of lithium from mineral resources: State-of-the-art and perspectives—A review. *Hydrometallurgy* **2019**, *189*, 105129. [CrossRef]
5. Yan, Q.X.; Li, X.H.; Wang, Z.X.; Wu, X.F.; Guo, H.J.; Hu, Q.Y.; Peng, W.J.; Wang, J.X. Extraction of valuable metals from lepidolite. *Hydrometallurgy* **2012**, *117*, 116–118. [CrossRef]
6. Zhang, X.; Tan, X.; Li, C.; Yi, Y.; Liu, W.; Zhang, L. Energy-efficient and simultaneous extraction of lithium, rubidium and cesium from lepidolite concentrate via sulfuric acid baking and water leaching. *Hydrometallurgy* **2019**, *185*, 244–249. [CrossRef]
7. Sun, C.Y.; Han, L.Z.; Song, J.W.; Zhen, G. The Study on Genetic Mineral Processing Engineering. *Nonferr. Met.* **2018**, *1*, 11. [CrossRef]
8. Takeda, H.; Burnham, C.W. Fluor-polylithionite: A lithium mica with nearly hexagonal $(Si_2O_5)_2$-ring. *Mineralogical. J.* **1969**, *6*, 102–109. [CrossRef]
9. Pandey, D.; Baronnet, A.; Krishna, P. Influence of stacking faults on the spiral growth of polytype structures in mica. *Phys. Chem. Miner.* **1982**, *8*, 268–278. [CrossRef]
10. Tressaud, A.; Labrugère, C.; Durand, E.; Serier, H.; Demyanova, L.P. Surface modification of phyllosilicate minerals by fluorination methods. *J. Vac. Sci. Technol. A* **2010**, *28*, 373–381. [CrossRef]
11. Hawthorne, F.C.; Sokolova, E.; Agakhanov, A.A.; Pautov, L.A.; Karpenko, V.Y. The Crystal Structure of Polylithionite-1M from Darai-Pioz, Tajikistan: The Role of Short-range Order in Driving Symmetry Reduction in 1M Li-rich Mica. *Can. Mineral.* **2019**, *57*, 519–528. [CrossRef]
12. Sartori, F.; Franzini, M.; Merlino, S. Crystal structure of a 2M2 lepidolite. *Acta. Crtstallogr. B* **1973**, *29*, 573–578. [CrossRef]
13. Guggenheim, S. Cation ordering in lepidolite. *Am. Mineral.* **1981**, *66*, 1221–1232.
14. Elmi, C.; Brigatti, M.F.; Guggenheim, S.; Pasquali, L.; Montecchi, M.; Nannarone, S. Crystal chemistry and surface configurations of two polylithionite-1M crystals. *Am. Mineral.* **2014**, *99*, 2049–2059. [CrossRef]
15. Chen, Y.; Chen, J.H.; Guo, J. A DFT study on the effect of lattice impurities on the electronic structures and floatability of sphalerite. *Miner. Eng.* **2010**, *23*, 1120–1130. [CrossRef]
16. Jiang, W.; Gao, Z.Y.; Sun, W.; Gao, J.D.; Hu, Y.H. A Density Functional Theory Study on the Effect of Lattice Impurities on the Electronic Structures and Reactivity of Fluorite. *Minerals* **2017**, *7*, 160. [CrossRef]
17. Dung, N.-T.; Cuong, N.-C.; Van, D.-Q. Study on the Effect of Doping on Lattice Constant and Electronic Structure of Bulk AuCu by the Density Functional Theory. *J. Multicsale Model.* **2020**, *11*, 2030001. [CrossRef]
18. Dong, Z.L.; Jiang, T.; Xu, B.; Hong, Z.; Zhang, B.S.; Liu, G.Q.; Li, Q.; Yang, Y.B. Density functional theory study on electronic structure of tetrahedrite and effect of natural impurities on its flotation property. *Miner. Eng.* **2021**, *169*, 106980. [CrossRef]
19. Rieder, M.; Cavazzini, G.; D'yakonov, Y.S.; Frank-Kamenetskii, V.A.; Gottardi, G.; Guggenheim, S.; Koval, P.V.; Mueller, G.; Neiva, A.M.R.; Radoslovich, E.W.; et al. Nomenclature of the micas. *Mineral. Mag.* **1999**, *63*, 267. [CrossRef]
20. Liu, J.; Gong, G.; Han, Y.; Zhu, Y. New Insights into the Adsorption of Oleate on Cassiterite: A DFT Study. *Minerals* **2017**, *7*, 236. [CrossRef]
21. Mayer, I. *Bond Order and Valence: Relations to Mulliken's Population Analysis*; Central Research Institute for Chemistry, Hungarian Academy of Sciences: Budapest, Hungary, 1984; Volume 26, pp. 151–154. [CrossRef]
22. Sun, C.Y.; Ying, W.Z. *Principle of Flotation of Silicate Minerals*; Science Publishers: Beijing, China, 2001; p. 476.

23. Zhang, H.T. Molecular Dynamics Simulation of Adsorption of Combined Dodecylamine and Oleic Acid Traps on Lithium Mica Surfaces. Master's Thesis, Jiangxi University of Science and Technology, Ganzhou, China, 2017.
24. Salmani, E.; Benyoussef, A.; Ez-Zahraouy, H.; Saidi, E.H.; Mounkachi, O. First-principles study and electronic structures of Mn-doped ultrathin ZnO nanofilms. *Chin. Phys. B* **2012**, *21*, 362–368. [CrossRef]
25. Robert, J.; Beny, J.; Beny, C.; Volfinger, M. Characterization of lepidolites by Raman and infrared spectrometries. I. Relationships between OH-stretching wavenumbers and composition. *Can. Miner.* **1989**, *27*, 225–235.
26. Li, S.P.; Zhang, J.M.; Abudukade, D.; Wang, Y.L. Research Status and Prospect of Lithium Mica Flotation Capture Agent. *Conserv. Util. Miner. Resour.* **2020**, *40*, 77–82. [CrossRef]

Disclaimer/Publisher's Note: The statements, opinions and data contained in all publications are solely those of the individual author(s) and contributor(s) and not of MDPI and/or the editor(s). MDPI and/or the editor(s) disclaim responsibility for any injury to people or property resulting from any ideas, methods, instructions or products referred to in the content.